We are IntechOpen, the world's leading publisher of Open Access books Built by scientists, for scientists

4,800
Open access books available

122,000
International authors and editors

135M
Downloads

Our authors are among the

154
Countries delivered to

TOP 1%
most cited scientists

12.2%
Contributors from top 500 universities

WEB OF SCIENCE™

Selection of our books indexed in the Book Citation Index in Web of Science™ Core Collection (BKCI)

Interested in publishing with us?
Contact book.department@intechopen.com

Numbers displayed above are based on latest data collected.
For more information visit www.intechopen.com

1

Experimental Results on Variable Structure Control for an Uncertain Robot Model

K. Bouyoucef[1], K. Khorasani[1] and M. Hamerlain[2]
[1]*Department of Electrical and Computer Engineering, Concordia University,*
[2]*Centre de Développement des Technologies Avancées (CDTA)*
[1]*Canada,* [2]*Algeria*

1. Introduction

To reduce computational complexity and the necessity of utilizing highly nonlinear and strongly coupled dynamical models in designing robot manipulator controllers, one of the solutions is to employ robust control techniques that do not require an exact knowledge of the system. Among these control techniques, the sliding mode variable structure control (SM-VSC) is one that has been successfully applied to systems with uncertainties and strong coupling effects.

The sliding mode principle is basically to drive the nonlinear plant operating point along or nearby the vicinity of the specified and user-chosen hyperplane where it 'slides' until it reaches the origin, by means of certain high-frequency switching control law. Once the system reaches the hyperplane, its order is reduced since it depends only on the hyperplane dynamics.

The existence of the sliding mode in a manifold is due to the discontinuous nature of the variable structure control which is switching between two distinctively different system structures. Such a system is characterized by an excellent performance, which includes insensitivity to parameter variations and a complete rejection of disturbances. However, since this switching could not be practically implemented with an infinite frequency as required for the ideal sliding mode, the discontinuity generates a chattering in the control, which may unfortunately excite high-frequency dynamics that are neglected in the model and thus might damage the actual physical system.

In view of the above, the SM-VSC was restricted in practical applications until progresses in the electronics area and particularly in the switching devices in the nineteen seventies. Since then, the SM-VSC has reemerged with several advances for alleviating the undesirable chatter phenomenon. Among the main ideas is the approach based on the equivalent control component which is added to the discontinuous component (Utkin, 1992; Hamerlain et al, 1997). In fact, depending on the model parameters, the equivalent control corresponds to the SM existence condition. Second, the approach studied in (Slotine, 1986) consists of the allocation of a boundary layer around the switching hyperplane in which the discontinuous control is replaced by a continuous one. In (Harashima et al, 1986; Belhocine et al, 1998), the gain of the discontinuous component is replaced by a linear function of errors. In (Furuta et

al, 1989), the authors propose a technique in which the sliding mode is replaced by a sliding sector.

Most recent approaches consider that the discontinuity occurs at the highest derivatives of the control input rather than the control itself. These techniques can be classified as a higher order sliding mode approaches in which the state equation is differentiated to produce a differential equation with the derivative of the control input (Levant & Alelishvili, 2007; Bartolini et al, 1998). Among them, a particular approach that is introduced in (Fliess, 1990) and investigated in (Sira-Ramirez, 1993; Bouyoucef et al, 2006) uses differential algebraic mathematical tools. Indeed, by using the differential primitive element theorem in case of nonlinear systems and the differential cyclic element theorem in case of linear systems, this technique transforms the system dynamics into a new state space representation where the derivatives of the control inputs are involved in the generalization of the system representation. By invoking successive integrations to recover the actual control the chattering of the so-called Generalized Variable Structure (GVS) control is filtered out.

In this paper, we present through extensive simulations and experimentations the results on performance improvements of two GVS algorithms as compared to a classical variable structure (CVS) control approach. Used as a benchmark to the GVS controllers, the CVS is based on the equivalent control method. The CVS design methodology is based on the differential geometry whereas the GVS algorithms are designed using the differential algebraic tools. Once the common state representation of the system with the derivatives of the control input is obtained, the first GVS algorithm is designed by solving the well-known sliding condition equation while the second GVS algorithm is derived on the basis of what is denoted as the hypersurface convergence equation.

The remainder of this chapter is organized as follows. After identifying experimentally the robot axes in Section 2, the procedure for designing SM-VSC algorithms is studied in Section 3. In order to evaluate the chattering alleviation and performance improvement, simulations and experimentations are performed in Section 4. Finally, conclusions are stated in Section 5.

2. Identification of robot manipulator axes

In this study, Generalized Variable Structure (GVSC) control techniques are implemented on the Robot Manipulator (RP41) as illustrated in Fig. 1-a. From the schematic that is depicted in Fig. 1-b, one can observe that the RP41 is a SCARA robot with four degrees of freedom. The three first joints (J1, J2, and J3) are rotoide while the fourth one (T) is prismatic. To each robot axis, one assigns a controller that uses only a measured angular signal that is generated by a shaft encoder via a 12 bit Analog/Digital converter. As far as control is concerned, it is digitized from 0 to 4096. As illustrated in Table 1, this interval corresponds to an analog input of the converter spanning from – 5 to + 5 Volts. In order to activate the DC drive of each robot joint, these low voltages are amplified by a power board to the range of -24 to +24 Volts.

In virtue of the robustness properties, uncertain linear models of the robot are obtained for the design of the SM-VS controllers. This section briefly presents the experimental identification of the three robot axes resulting in a suitable second order linear model for each manipulator axis.

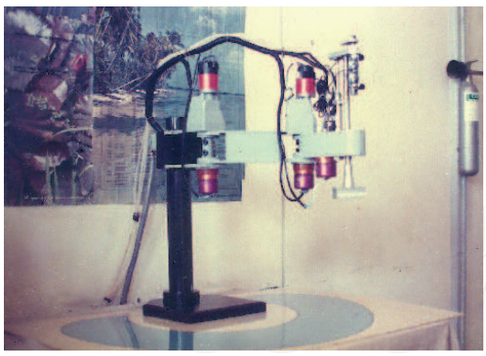

(a) The SCARA Robot RP41

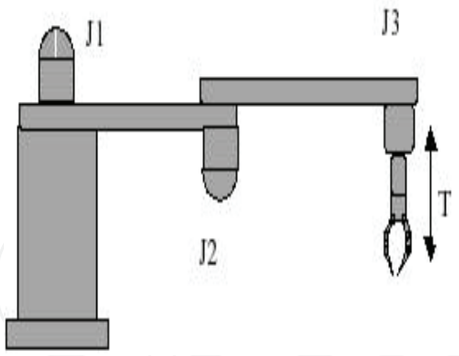

(b) Schematic of the SCARA RP41 mechanism

Figure 1. The SCARA Robot Manipulator (RP 41), *(Centre de Développement des Technologies Avancées, Algiers)*

Digital controller output	D/A Converter output [volts]	Robot DC motors input [volts]
0	+5	+24
2048	0	0
4096	-5	-24

Table 1. Digital and analog control ranges

For further explanations on the identification of the arm axes, the reader can refer to our previous investigations (Youssef et al, 1998). The complete Lagrange formalism-based dynamic model of the considered SCARA robot has been experimentally studied in (Bouyoucef et al, 1998), in which the model parameters are identified and then validated by using computed torque control algorithm. The well-known motion dynamics of the three joints manipulator is described by equation (1)

$$M(q)\,.\,\ddot{q} + h(q\,,\dot{q}) + g(q) = u \tag{1}$$

Where $q, \dot{q}, \ddot{q} \in R^3$ are the vectors of angular position, velocity and acceleration, respectively, $M(.) \in R^{3x3}$ is the symmetric positive definite inertia matrix, $h(.) \in R^{3x3}$ is the coefficient matrix of the centripetal and Coriolis torques, $g(.) \in R^3$ is the vector of the gravitational torques, and $u(.) \in R^3$ is the vector of torques applied to the joints of the manipulator.

As developed in (Youssef et al, 1998), considering the diagonal elements preponderance of the non singular matrix $M(q)$, and replacing $h(q, \dot{q})$ and $g(q)$ by $C(q, \dot{q})\dot{q}$ and $G(q)q$, respectively, $M^{-1}(q)\,C(q, \dot{q})$, $M^{-1}(q)\,G(q)$ and $M^{-1}(q)$ by A_1, A_0 and B, respectively, equation (1) can be written as follows:

$$\ddot{q} + A_1\dot{q} + A_0 q = B\,u \tag{2}$$

where each of the diagonal matrices A_0, A_1 and B contains the dynamic parameters of the three robot axes for the angle, rate and control variables, respectively. On the basis of the

plant input/output data, the parametric identification principle consisting of the estimation of the model parameters according to a priori user-chosen structure was performed. Adopting the ARX (Auto regressive with exogenous input) model, and using the Matlab software, the off-line identification generated the robot parameters according to model (2), which are illustrated in Table 1.

$A_0 = diag\begin{bmatrix} -5.4 & -2.41 & -117 \end{bmatrix}$
$A_1 = diag\begin{bmatrix} 560.7 & 200 & 413.5 \end{bmatrix}$
$B = diag\begin{bmatrix} 0.5 & 0.65 & 7.5 \end{bmatrix}$

Table 1. The identification of the robot parameters corresponding to model (2)

Note that in compliance with model (2), the obtained parameters correspond to the robot model that is used in the CVS control approach, which constitutes in this study as the benchmark to our proposed GVS control approaches. In order to implement GVS approaches, model (2) is not suitable since it doesn't exhibit the derivatives of the control, however, model (3) that contains the zeros dynamics is utilized instead, namely

$$\ddot{q} + A_1\dot{q} + A_0 q = B_1\ \dot{u} + B_0 u \tag{3}$$

Using the same identification procedure as before, the parameters for model (3) are now given in Table 2.

$A_0 = diag\begin{bmatrix} -2.4 & -2.965 & -13.258 \end{bmatrix}$
$A_1 = diag\begin{bmatrix} 201 & 200.92 & 213.92 \end{bmatrix}$
$B_0 = diag\begin{bmatrix} 0.65 & 0.67 & 0.61 \end{bmatrix}$
$B_1 = diag\begin{bmatrix} 0.041 & 0.004 & 0.006 \end{bmatrix}$

Table 2. The identification of the robot parameters corresponding to model (3)

3. Sliding mode-based variable structure control strategy

The CVS control has been used for a number of years. The switching occurs on the control variable, and this is discussed in the next subsection in the context of differential geometry and constitutes in this study as the benchmark to GVS control approaches. Recently the GVS scheme was introduced in (Fliess, 1990) where the switching occurs on the highest

derivative of the control input. The GVS analysis and design are studied in the context of the differential algebra. In subsection 3.2, we design two GVS control approaches, the first GVS approach is designed by solving the well-known sliding condition equation, while the second GVS approach is derived on the basis of what is denoted as the hypersurface convergence equation.

3.1 Classical variable structure control in the differential geometry context

Consider the nonlinear dynamical system in which the time variable is not explicitly indicated, that is

$$\frac{dx}{dt} = f(x) + g(x)U \tag{4}$$

where $x \in X$ is an open set of R^n, $f(x) = [f_1, f_2, \cdots, f_n]^T$ and $g(x) = [g_1, g_2, \cdots, g_n]^T$ are vector fields defined on R^n with $g(x) \neq 0 \ \ \forall\, x \in X$, and the control is defined so that $U : R^n \rightarrow R$.

Assume a hypersurface $S = \left\{ x \in R^n : S(x) = 0 \right\}$ is denoted as the 'sliding surface' on which discontinuous control functions of the type

$$U = \begin{cases} U^+(x) & \text{if} \quad S(x) > 0 \\ U^-(x) & \text{if} \quad S(x) < 0 \end{cases} \tag{5}$$

make the surface attractive to the representative point of the system such that it slides until the equilibrium point is reached. This behavior occurs whenever the well-known sliding condition $S\dot{S} < 0$ is satisfied (Utkin, 1992).

Using the directional derivative $L_h \sigma$, this condition can be represented as

$$\begin{cases} \lim\limits_{S \to 0^+} L_{f+gU^+} S < 0 \\ \lim\limits_{S \to 0^-} L_{f+gU^-} S > 0 \end{cases} \tag{6}$$

or by using the gradient ∇ of S and the scalar product $<.,.>$ as

$$\begin{cases} \lim\limits_{S \to 0^+} \left\langle \nabla S, f + g \cdot U^+ \right\rangle < 0 \\ \lim\limits_{S \to 0^-} \left\langle \nabla S, f + g \cdot U^- \right\rangle > 0 \end{cases} \tag{7}$$

A geometric illustration of this behavior is shown in Figure 2, in which the switching of the vector fields occurs on the hypersurface $S(x) = 0$.

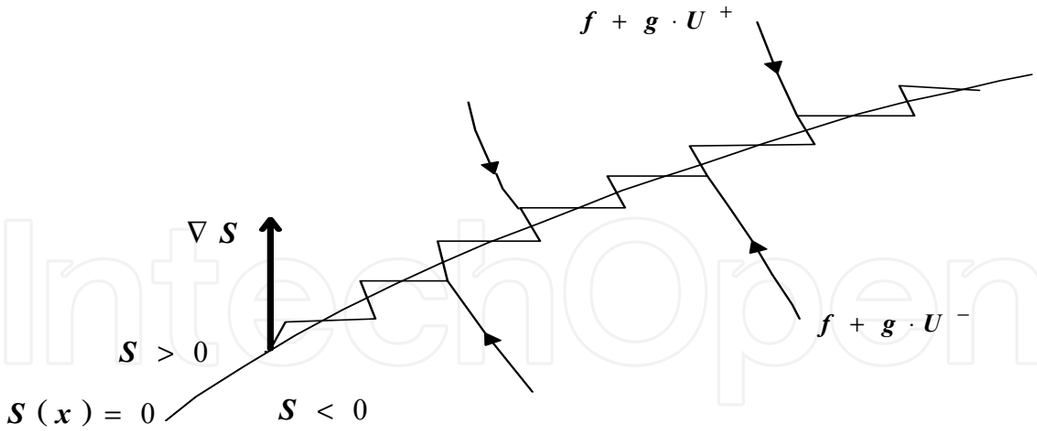

Figure 2. The geometric illustration of the sliding surface and switching of the vector fields on the hypersurface $S(x)=0$

Depending on the system state with respect to the surface, the control is selected such that the vector fields converge to the surface. Specifically, using the equivalent control method, the classical variable structure control law can be finally expressed as a sum of two components as follows,

$$U = U_{eq} + \delta U \tag{8}$$

where the equivalent control component U_{eq} is derived for the ideal sliding mode so that the previously defined hypersurface is a local invariant manifold. Therefore, if $S(x)=0$,

$$L_{f+g\cdot U_{eq}} S = \left\langle \nabla S, f + g \cdot U_{eq} \right\rangle = 0, \text{ then}$$

$$U_{eq} = -\frac{\left\langle \nabla S, f \right\rangle}{\left\langle \nabla S, g \right\rangle} = -\frac{L_f S}{L_g S} \tag{9}$$

whereas the second component corresponds to the discontinuous control so that $\delta U = -Msign(S)$ where the gain *M* should be chosen to be greater than the perturbation signal amplitude. A typical control U (dotted line), and its components U_{eq} (solid line), and δU (dashed line) are illustrated in Fig. 3. It can be seen that the state of the discontinuous component δU changes from continuous and positive to discontinuous with variable sign. This change coincides to the first crossing of the surface $S(x)=0$. In compliance with the equivalent control component that is always positive, it also switches since it is derived by using the derivative of the surface but with a small amplitude. The switching of the equivalent control component occurs one iteration later than the discontinuous component switching. The control U that is always postive corresponds to the geometric sum of both U_{eq} and δU.

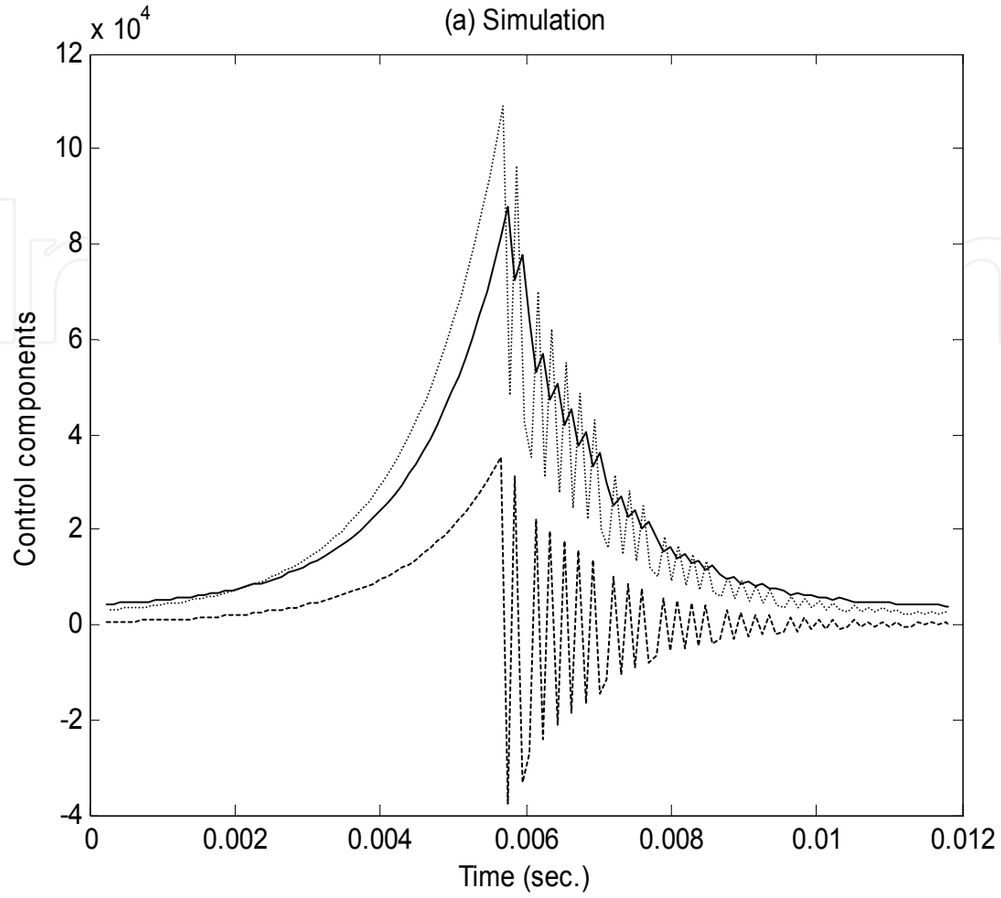

Figure 3. The control and its equivalent and discontinuous components (U dotted line, U_{eq} solid line, and δU dashed line)

3.2 Generalized variable structure control

In the context of differential algebra, and under the existence conditions of the differential primitive element for nonlinear systems, or cyclic element in the case of linear systems, the elimination of the state in the original Kalman state representation leads to the pair Generalized Control Canonical Form (GCCF) and Generalized Observable Canonical Form (GOCF). By associating for example the output equation $y = h(x)$ to the given state equation (4), the elimination of x in both state and output equations leads to the following differential equation:

$$\varsigma(y, \dot{y}, \cdots, y^{(d-1)}, y^{(d)}, u, \dot{u}, \cdots, u^{(\alpha)}) = 0 \tag{10}$$

where $\alpha = d - r$ is a strictly positive integer related to the relative degree r of the output function y with respect to the scalar input u. The integer d is defined such that the rank condition (11) should be satisfied

$$rank\,\frac{\delta(h,\dot{h},\cdots,h^{(d-1)})}{\delta x}=rank\,\frac{\delta(h,\dot{h},\cdots,h^{(d-1)},h^{(d)})}{\delta x} \tag{11}$$

Defining a new variable $\eta_i = y^{i-1}$ where $i=1,\cdots,\ d$ and assuming that the Jacobian $\frac{\delta(\xi)}{\delta(y)^{(d)}}$ is locally nonsingular, the transformation from the implicit input-output representation to the locally explicit GOCF given by (12) may be accomplished as follows:

$$(GOCF)\begin{cases}\dot{\eta}_i=\eta_{i-1};\quad (i=1,2,\cdots,n-1)\\ \dot{\eta}_n=\varsigma(\eta,u,\dot{u},\cdots,u^{(\alpha)})\\ y=\eta_1\end{cases} \tag{12}$$

For tracking control purposes, one considers a reference trajectory $W_R(t)=[y_R(t),\dot{y}_R(t),...,y_R^{(n-1)}(t)]^T$ and defines the tracking error vector $e(t)=[e_1,e_2,...,e_n]^T=\eta(t)-W_R(t)$ such that

$$\begin{cases}e_1=y-y_R\\ e_i=e_1^{(i-1)}=\eta_i-y_R^{(i-1)},\quad i=2,\cdots,n\end{cases} \tag{13}$$

The system (12) is now rewritten in the error coordinates as follows:

$$\begin{cases}\dot{e}_i=e_{i+1},\quad (i=1,\cdots,n-1)\\ \dot{e}_n=\varsigma(W_R(t)+e(t),u,\dot{u},...,u^{(\alpha)})-y_R^{(n)}(t)\\ e_1=y-y_R\end{cases} \tag{14}$$

It is worth mentioning that the state representation of the system obtained with the derivatives of the control input constitutes the core of the GVS control design procedure. Using the common state representation (14), several GVS control approaches can be studied. Three approaches are considered for deriving the GVS control algorithm, namely

a. by solving the well-known sliding condition $S\dot{S}<0$ after substitution of (14) (the reader can refer to (Belhocine et al, 1998) for more details and experimental results about this approach) ;
b. by using what is denoted as the hypersurface convergence equation (15),

$$\frac{dS}{dt}+\mu\,S=-\mu\,\Omega sign(S) \tag{15}$$

where μ and Ω are positive design parameters, and $sign\,(S)$ is the signum function, and
c. by considering the following feedback control that is introduced in (Messager, 1992).

$$\varsigma\left(\eta_1,...,\eta_n,u,\dot{u},...,u^{(\alpha)}\right)=\sum_{i=1}^{n}\overline{a}_i\eta_i+\sum_{i=1}^{\alpha}\overline{b}_i v_i \tag{16}$$

where $\eta=\eta_1,...,\eta_n$, $v=v_1,\cdots,v_\alpha$ is the new input, and $\overline{a}_i$, $\overline{b}_i$ are chosen according to the stability of the resulting system.

In this study, a linear hypersurface can be defined in the error state space $e(t)$ as

$$S(t)=e_n+\sum_{i=1}^{n-1}s_i e_i \tag{17}$$

The representative operating point of the control system, whose structure switches on the highest derivative of the input as shown in Fig. 4, slides on the defined surface $S(t)=0$ until the origin, whenever the existence condition $S\dot{S}<0$ holds.

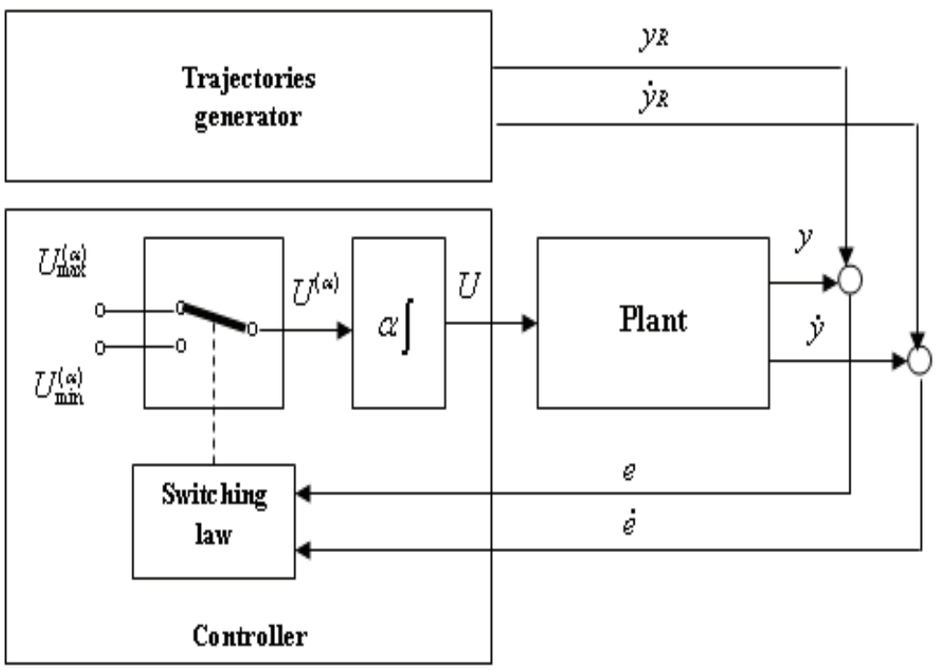

Figure 4. The switching principle in the GVS control system

3.3 The generalized variable structure control controller design

Through its robustness property, the GVS is insensitive to the interactions between manipulator axes which can be regarded as disturbances. Therefore, for the considered MIMO robotic system, the controller can be designed as a SISO system, in addition, the control design does not require an accurate model. As mentioned earlier, in order to design the aforementioned GVS control laws, one starts by deriving the common state

representation of the system with the derivatives of the control input by using the second-order linear model (3) that was obtained in robot axes identification section.
However, let us rewrite for each arm axis the second-order linear model (3) where q , $\dot{q}$, and $\ddot{q}$ are the joint angles, angular rates, and accelerations, respectively,

$$\ddot{q}_i + a_{1i}\dot{q}_i + a_{0i}q_i = b_{0i}u_i + b_{1i}\dot{u}_i; \quad (i = 1, \cdots, 3) \tag{18}$$

Let us now introduce a new set of state variables that are given according to

$$\begin{cases} \eta_{1i} = q_i \\ \eta_{2i} = \dot{q}_i = \dot{\eta}_{1i} \\ \dot{\eta}_{2i} = \ddot{q}_i \end{cases} \tag{19}$$

Therefore, by substituting the new variables (19) into (18), the GOCF representation is obtained as follows:

$$(GOCF)\begin{cases} \dot{\eta}_{1i} = \eta_{2i} \\ \dot{\eta}_{2i} = -a_{0i}\eta_{1i} - a_{1i}\eta_{2i} + b_{0i}u_i + b_{1i}\dot{u}_i \\ q_i = \eta_{1i} \end{cases} \tag{20}$$

Now to consider the control system design in the error state space, let us define the error variables as shown in (21):

$$\begin{cases} e_{1i} = \eta_{1i} - \eta_{iref} \\ \dot{e}_{1i} = e_{2i} = \dot{\eta}_{1i} - \dot{\eta}_{iref} = \eta_{2i} - \dot{\eta}_{iref} \\ \dot{e}_{2i} = \dot{\eta}_{2i} - \ddot{\eta}_{iref} \end{cases} \tag{21}$$

where η_{iref} is the angular reference corresponding to the robot axis i . By substituting these into the GOCF model (20), we get

$$(GOCF)\begin{cases} \dot{e}_{1i} = e_{2i} \\ \dot{e}_{2i} = -a_{0i}e_{1i} - a_{1i}e_{2i} + b_{0i}u_i + b_{1i}\dot{u}_i - a_{0i}\eta_{iref} - a_{1i}\dot{\eta}_{iref} - \ddot{\eta}_{iref} \\ q_i = e_{1i} + \eta_{iref} \end{cases} \tag{22}$$

Following the GOCF representation that is obtained in the error state space and is given by (22), the derivation of two GVS control approaches are performed for the same linear switching surface that is given by (17). In fact, the objective is to ensure robustness of the closed-loop system against uncertainties, unmodeled dynamics and external perturbations. This will be the case provided that for the above system (22), a sliding mode exists in some neighborhood of the switching surface (23) with intersections that are defined in the same space of which function (23) is characterized, that is

$$S_i(t) = s_{1i}e_{1i} + \dot{e}_{1i} = s_{1i}e_{1i} + e_{2i}; \quad (i = 1, \cdots, 3) \tag{23}$$

with the derivatives as given by

$$\dot{S}_i(t) = s_{1i}\dot{e}_{1i} + \dot{e}_{2i} = s_{1i}e_{2i} + \dot{e}_{2i}; \quad (i = 1, \cdots, 3) \tag{24}$$

where s_{1i} designates positive parameters corresponding to each robot axis.
Let us designate the first GVS control approach as GVS1 which is derived by solving the sliding existence condition $S\dot{S} < 0$ in which the GOCF model (22) is substituted, that is

$$\begin{cases} \dot{u}_i = b_{1i}^{-1}[-b_{0i}u_i + a_{0i}e_{1i} + (a_{1i} - s_{1i})e_{2i} \\ + a_{0i}\eta_{iref} + a_{1i}\dot{\eta}_{iref} + \ddot{\eta}_{iref} - M_i sign(S_i)] \end{cases} \tag{25}$$

The second GVS control approach that is designated as GVS2 is derived by imposing that the defined surfaces are solutions to the differential equations given by (26):

$$\frac{dS_i}{dt} + \mu_i S_i = -\mu_i \Omega_i sign(S_i); \quad (i = 1, \cdots, 3) \tag{26}$$

where the positive design parameters μ and Ω are chosen such that the dynamics described by the differential equation (27) is asymptotically stable. The latter can be written in an explicit form by substituting (23) and (24) into (26), that is

$$\dot{e}_{2i} = -s_{1i}e_{2i} - \mu_i(\Omega_i sign(S_i) + S_i); \quad (i = 1, \cdots, 3) \tag{27}$$

Now, let us consider (27) as a feedback control to model (22), that is

$$\begin{cases} \dot{e}_{2i} = -a_{0i}e_{1i} - a_{1i}e_{2i} + b_{0i}u_i + b_{1i}\dot{u}_i - a_{0i}\eta_{iref} - a_{1i}\dot{\eta}_{iref} - \ddot{\eta}_{iref} \\ \quad = -(s_{1i} + \mu_i)e_{2i} - \mu_i s_{1i}e_{1i} - \mu_i \Omega_i sign(S_i) \\ \quad = \sum_{j=1}^{2} \overline{a}_{ji}e_{ji} + v_i \end{cases} \tag{28}$$

One can observe that the above is the feedback control given by (16), where $\sum_{j=1}^{2} \overline{a}_{ji}e_{ji} + v_i$ is the resulting system corresponding to each axis, and the coefficients $\overline{a}_{ji}$ are chosen such that stability of the closed-loop system is ensured. Consequently, the above feedback control leads to the control law specified below:

$$\begin{cases} \dot{u}_i = b_{1i}^{-1}[b_{0i}u_i + (a_{0i} - \mu_i s_{1i})e_{1i} + (a_{1i} - s_{1i} - \mu_i)e_{2i} \\ \quad + a_{0i}\eta_{iref} + a_{1i}\dot{\eta}_{iref} + \ddot{\eta}_{iref} - \mu_i \Omega_i sign(S_i)] \end{cases} \tag{29}$$

Governed by integration of (29), the signal u constitutes the control variable that is sent to the plant and represents the advantages of the chattering alleviation scheme in comparison to the approach given by (16). This is possible since the differential equation permits one to better adjust the convergence of $S_i(t)$.

4. Simulations and experimental results

The simulations and experimentations presented in this section are conducted to demonstrate the effectiveness of the results obtained on the SCARA robot manipulator as illustrated in Fig. 1-a by using the two generalized variable control approaches designated as GVS1 and GVS2 in the previous section. These two GVS approaches are compared to the CVS control approach in terms of performance improvement and chattering alleviation capability.

Simulations are first performed on the model of the robot axis 3, for a step input, which show the benefits of the GVS control approaches and particularly the GVS2 in terms of performance and chattering alleviation by comparison with the CVS control approach. Subsequently, a set of experimentations are conducted on the three axes of the robot to confirm for a step input the simulation results as well as the robustness of the proposed algorithm. Note that in the comparative study only the results corresponding to the rotoide axis 3 are presented since its dynamics is faster than those of the two other axes 2 and 3 and the end effector that it supports.

Furthermore, the experimental results corresponding to the three axes that are obtained in the tracking mode are also presented.

In the simulation presented below, (a) the sampling time is set to $1ms$, (b) the control parameters corresponding to the CVS are designed to be $s_1 = 80$, $M = 5.10^3$, and those of the GVS1 are set so that $s_1 = 100$, $M = 2.10^5$; whereas those of the GVS2, they are designed to be $s_1 = 150$, $\mu = 1000$, and $\Omega = 50$; and (c) the reference angles are set to $q_{ref} = 2.1\,rad$. In the simulation results presented in Fig. 5 (a), one can observe that corresponding to step responses of the CVS (solid blue line), the GVS1 (dotted red line) and the GVS2 (dashed green line) on one hand the axis angle converges to its reference by using any control approach, and on the other hand, the system performance is improved, particularly in terms of the system response time when the GVS2 is used. The last three rows of Fig. 5 are dedicated to the control and the phase plane characteristics of the CVS, GVS1 and GVS2, respectively. The control characteristics are shown in the left hand side column while the characteristics of the phase plane are illustrated in the right hand side column. As far as the control characteristics (b), (d), and (f) are concerned the alleviation of the chattering phenomenon is readily validated when the GVS control approaches are used. This alleviation is more significant by using the GVS2 approach. However, the price that is paid for this improvement is in the increase of the control effort. From the plots in Fig. 5(c), (e), (g), one can observe that the behaviour of the system consists of first being attracted to the surface and then sliding on the surface with a slope s_{1i} linearly towards the origin. Furthermore, note that by increasing the design parameter s_{1i}, one improves the performance of the control system.

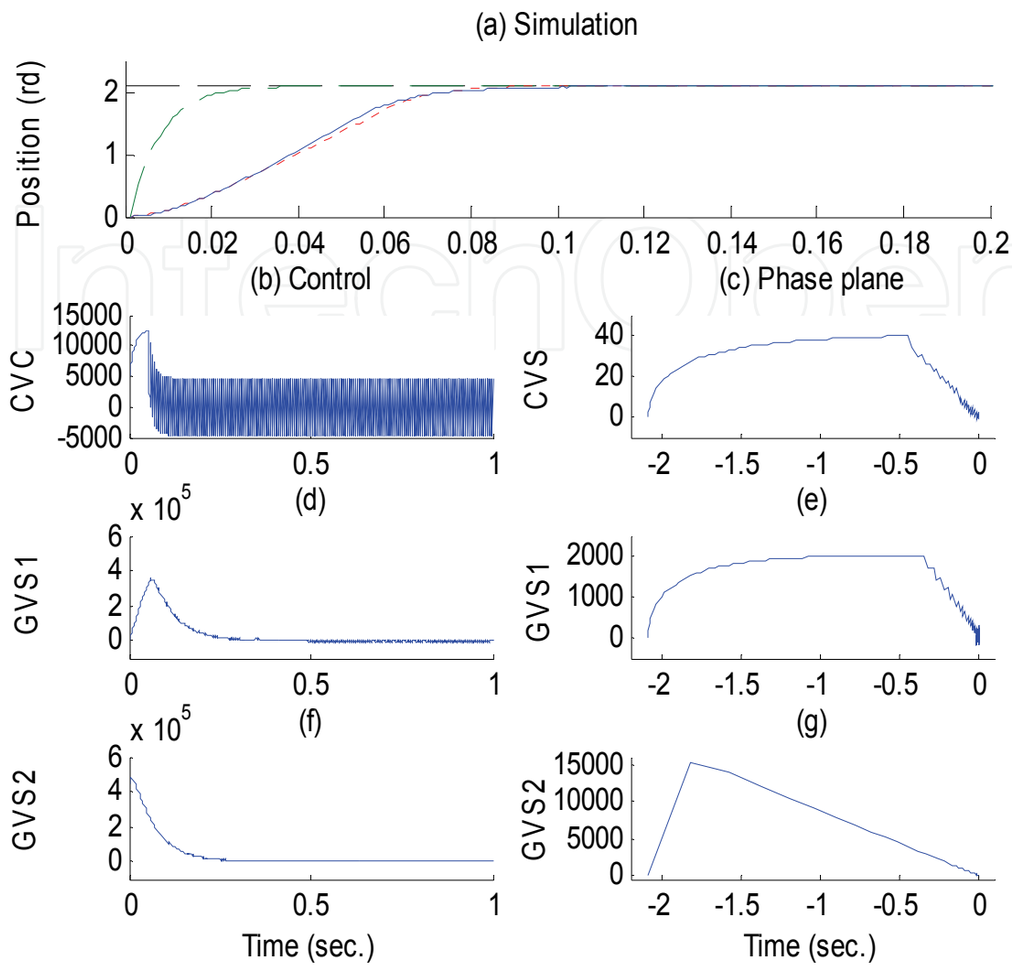

Figure 5. Comparative simulations of the GVS1, GVS2, and CVS controllers on the robot axis model

After designing the CVS and GVS controllers on the basis of a three axes model parameters discussed in the identification section, the experimental implementation results of the three robot axes are illustrated in Figs. 6–10.

In the experimentations presented below, (a) the sampling time is set to $5ms$, (b) the best controller parameters are: $s_{1i}=[20\ \ 80\ \ 40]$ and $M_i=[65\ \ 10^3\ \ 200]$ for the CVS, and $s_{1i}=[80\ \ 60\ \ 5]$ and $M_i=[1500\ \ 500\ \ 25]$ for the GVS1 whereas for the GVS2 they are set to $s_{1i}=[120\ \ 60\ \ 5]$, $\mu_i=[60\ \ 40\ \ 80]$ and $\Omega_i=[20\ \ 10\ \ 0.1]$, with $i=1,\cdots,3$ corresponding to the robot axes, and (c) the three axes initial angles are set to $q_{initial}=[0.92\ \ 0.92\ \ 0.52]$ radians and the final angles are set to $q_{final}=[2.09\ \ 2.09\ \ 2.09]$ radians as illustrated in Table 4.

The first experiment corresponding to Figs. 6 and 7 is conducted to confirm the simulation results that are illustrated in Fig. 5. These results are obtained without a payload and

external disturbances using step reference inputs and the initial and final angles as stated earlier. Figure 6(a) shows that the fastest step response is obtained by using the GVS2 approach and where the GVS1 approach step response is faster than that of the CVS approach. In addition, Fig. 6(b), (d), (f), that correspond to the control characteristics of the CVS, GVS1 and GVS2, respectively, demonstrate the chattering alleviation of the GVS control approaches. In order to show this improvement, the three control characteristics in Fig. 6 are zoomed in the steady state (i.e., 1s $\leq$ time $\leq$ 3s) and are depicted in Fig. 7. Indeed, one can clearly observe that the GVS1 control approach illustrated by graph (b) alleviates the chattering better than the CVS control that is given by graph (a). However, our best results are obtained with the GVS2 control approach as shown in graph (c).
The diminishing of the chattering is also visible through the smooth plots in Fig. 6(e) and (g) corresponding to the phase plane of GVS1 and GVS2 in comparison to the CVS that is shown in Fig. 6(c). From the above comparative results, it can be seen that the GVS2 control approach enjoys the best capabilities for chattering alleviation and performance improvement in comparison to the CVS and GVS1 control approaches.

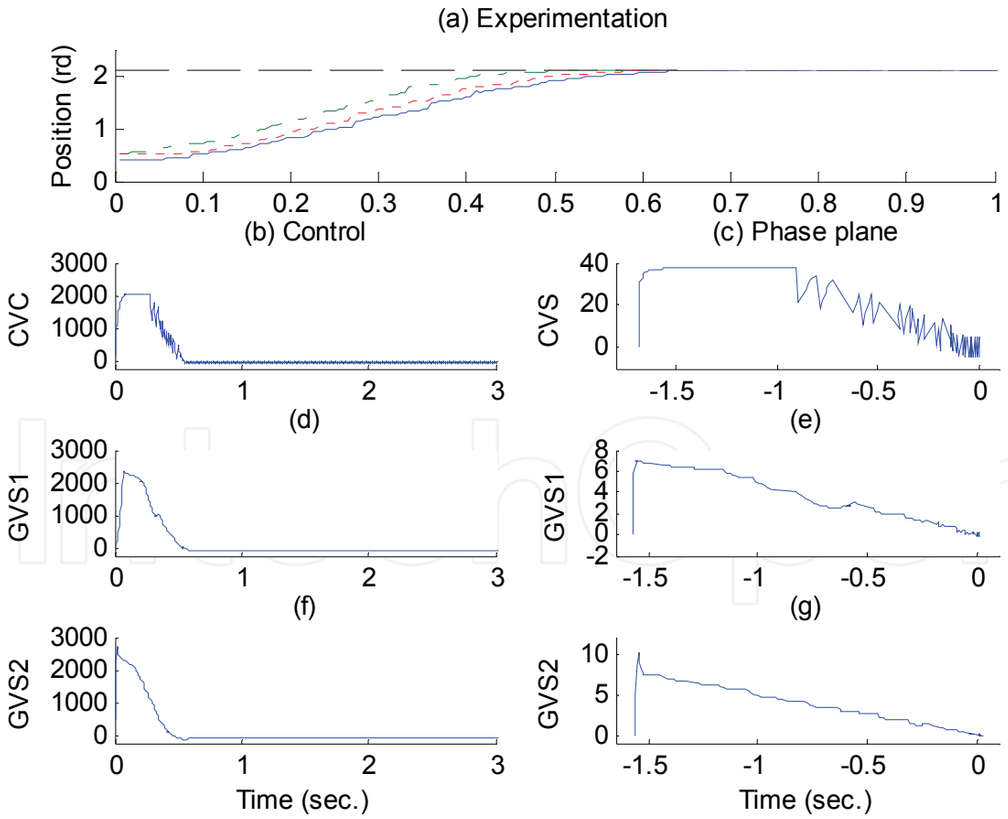

Figure 6. Comparative experimental results of the GVS1, GVS2, and CVS controllers for the robot axis model

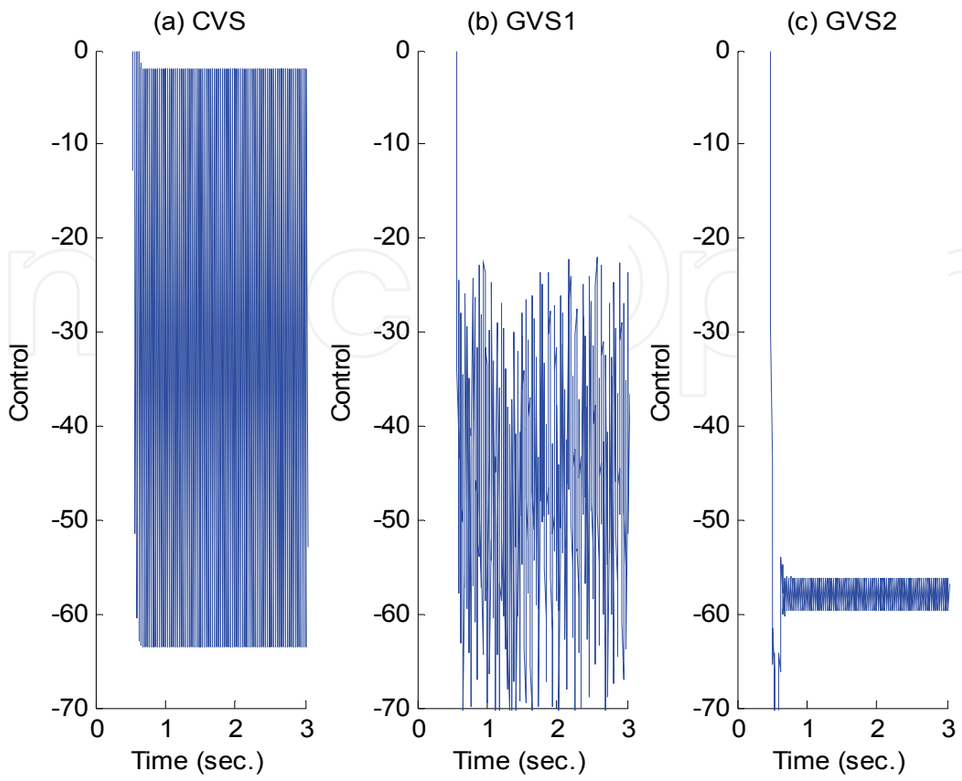

Figure 7. The zoomed graphs of the control characteristics shown in Fig. 6(b), (d), and (f) in the steady state

The second experimentation is operated in the tracking mode on our SCARA robot in order to show the robustness properties of our proposed GVS2 controller to an external disturbance and parameter variations caused by a 900 g payload. As shown in the following algorithm, depending on the difference absolute value between the final and the initial axis angles, the reference trajectory (Belhocine et al, 1998) applied to each robot axis has a trapezoidal or triangular profile, whose cruising velocity and acceleration amplitude are presented in Table 4. Note that, the initial and final configurations of the reference trajectory given in Table 4 correspond to the same initial and final angles that are used in the first experimentation conducted in the regulation mode.

Note also that for this experimentation, the sampling period for the new reference trajectory is $35ms$ whereas the regulation sampling time is kept at $5ms$, as in the first experimentation.

Axis	$q_i(rd)$	$q_f(rd)$	V (rd/s)	A (rd/s^2)
1,2	0.92	2.09	0.35	0.35
3	0.52	2.09	3.00	3.00

Table 4. The reference trajectory settings

Algorithm generating the reference trajectories:

If $\left|q_f - q_i\right| \geq \frac{V^2}{A}$

then use the trapezoidal profile

$$t_{acc} = \frac{V}{A}$$

$$t_{vit} = \left(\frac{1}{V}\right)\left|q_f - q_i\right| - t_{acc}$$

$$t_{tot} = t_{vit} + 2t_{acc}$$

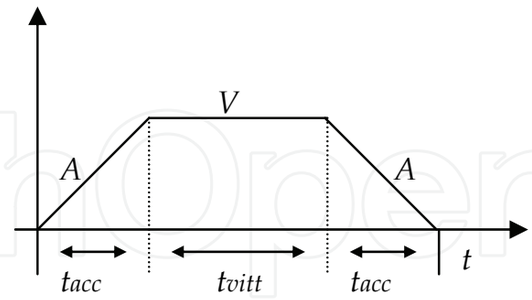

Otherwise use the triangular profile

$$t_{acc} = \frac{V}{A}$$

$$t_{vit} = 0$$

$$V = \left(\left|q_f - q_i\right|.A\right)^{\frac{1}{2}}$$

$$t_{tot} = 2t_{acc}$$

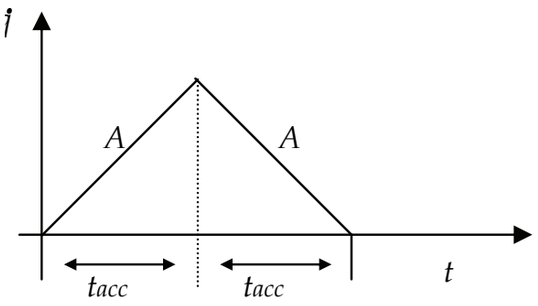

where q_i and q_f are the initial and final angles of each axis, respectively, V, A are the cruising velocity and acceleration amplitude, and $t_{acc}, t_{vitt}, t_{tot}$ are the accelaration, constant velocity and total times. Moreover, in compliance with Figs. 8-10 corresponding to the results obtained on axes 1-3, respectively, by using our proposed GVS2 in the tracking mode, one can see through the graphs (a) and (b) of each figure how the robot angles and rates follow the reference trajectories even when a strong disturbance and payload are added. It can also be noted that the spikes present in the velocity characteristics are due to the fact that the velocity is not measured but computed. In addition, one can observe that the control characteristics depicted by graph (c) of each figure is chattering-free.

5. Conclusion

Motivated by the VSC robustness properties, uncertain linear models of a robot are obtained for design of VS-based controllers. In this study, we presented through extensive simulation and experimentations results on chattering alleviation and performance improvements for two GVS algorithms and compared them to a classical variable structure (CVS) control approach. The GVS controllers are based on the equivalent control method. The CVS design methodology is based on the differential geometry whereas the GVS controllers are designed by using the differential algebraic tools. The results obtained from implementation of the above controllers can be summarized as follows: a) the GVS controllers do indeed filter out the control chattering characteristics and improve the system performance when compared to the CVS approach; b) the filtering and performance improvements are more clearly evident by using the GVS algorithm that is obtained with the hypersurface

convergence equation; and c) in the tracking mode, in addition to the above improvements, the GVS control also enjoys insensitivity to parameter variations and disturbance rejection properties.

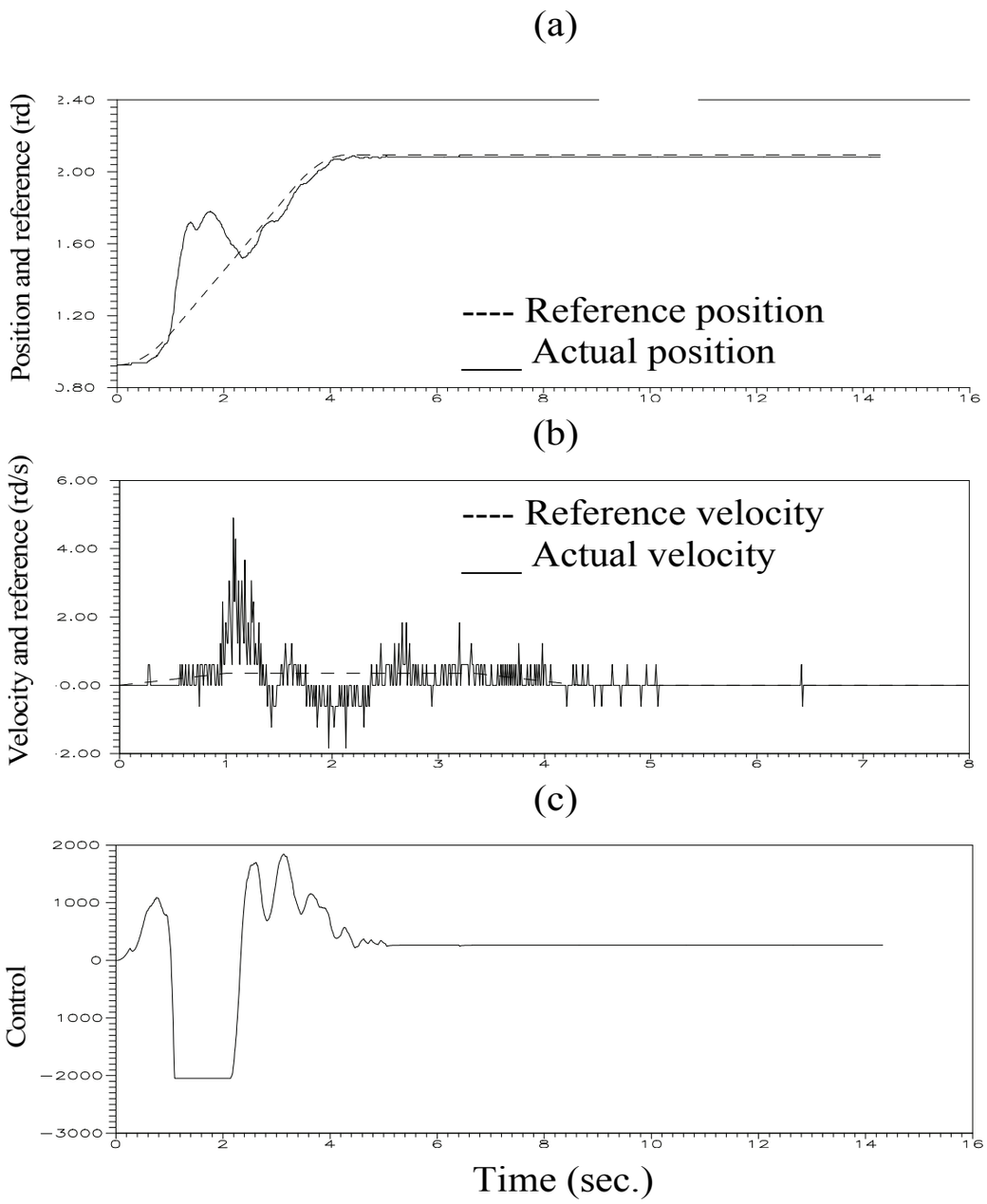

Figure 8. Experimental results obtained in the tracking mode using our proposed GVS2 controller on axis 1 in presence of 900g payload and external disturbance

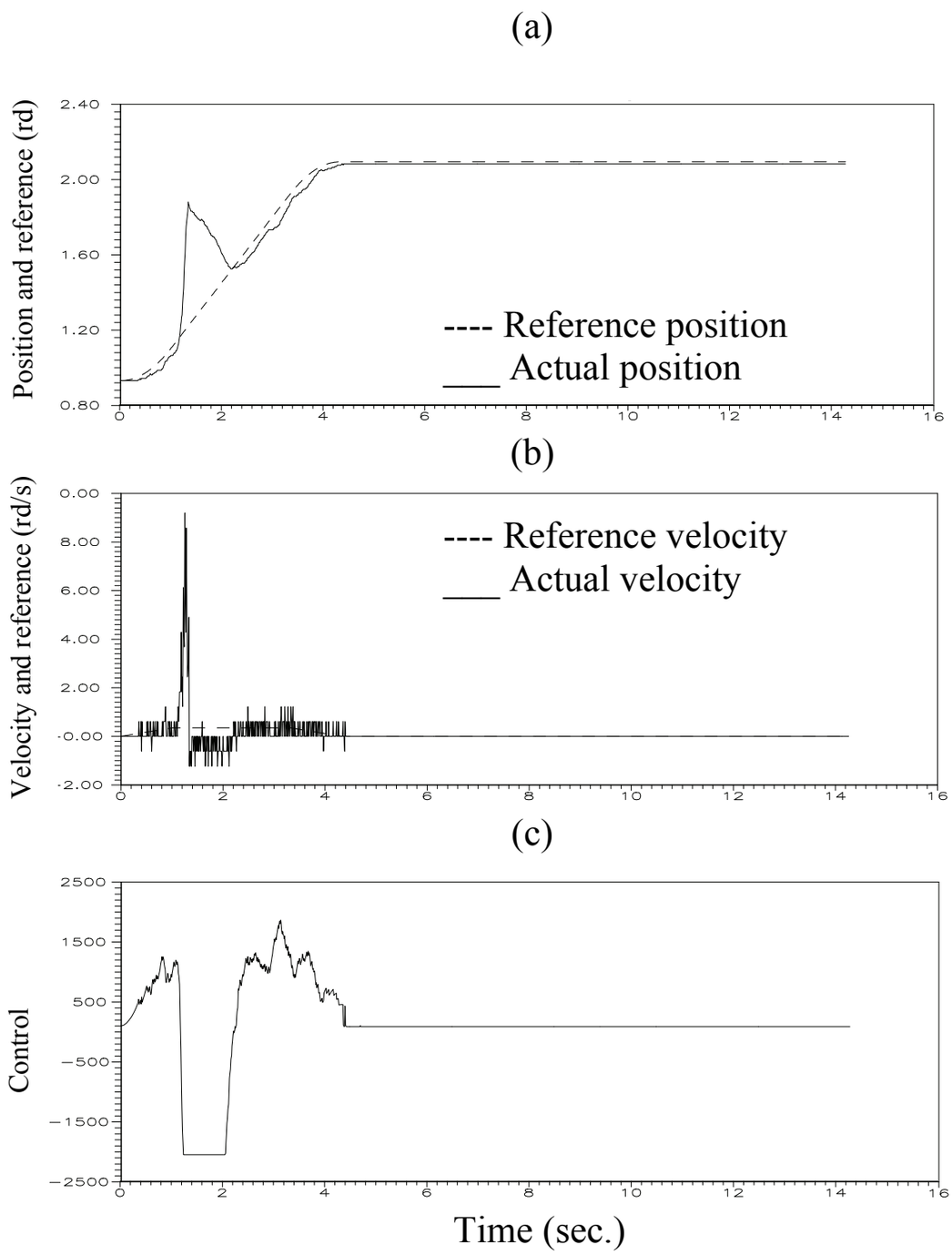

Figure 9. Experimental results obtained in the tracking mode using our proposed GVS2 controller on axis 2 in presence of 900g payload and external disturbance

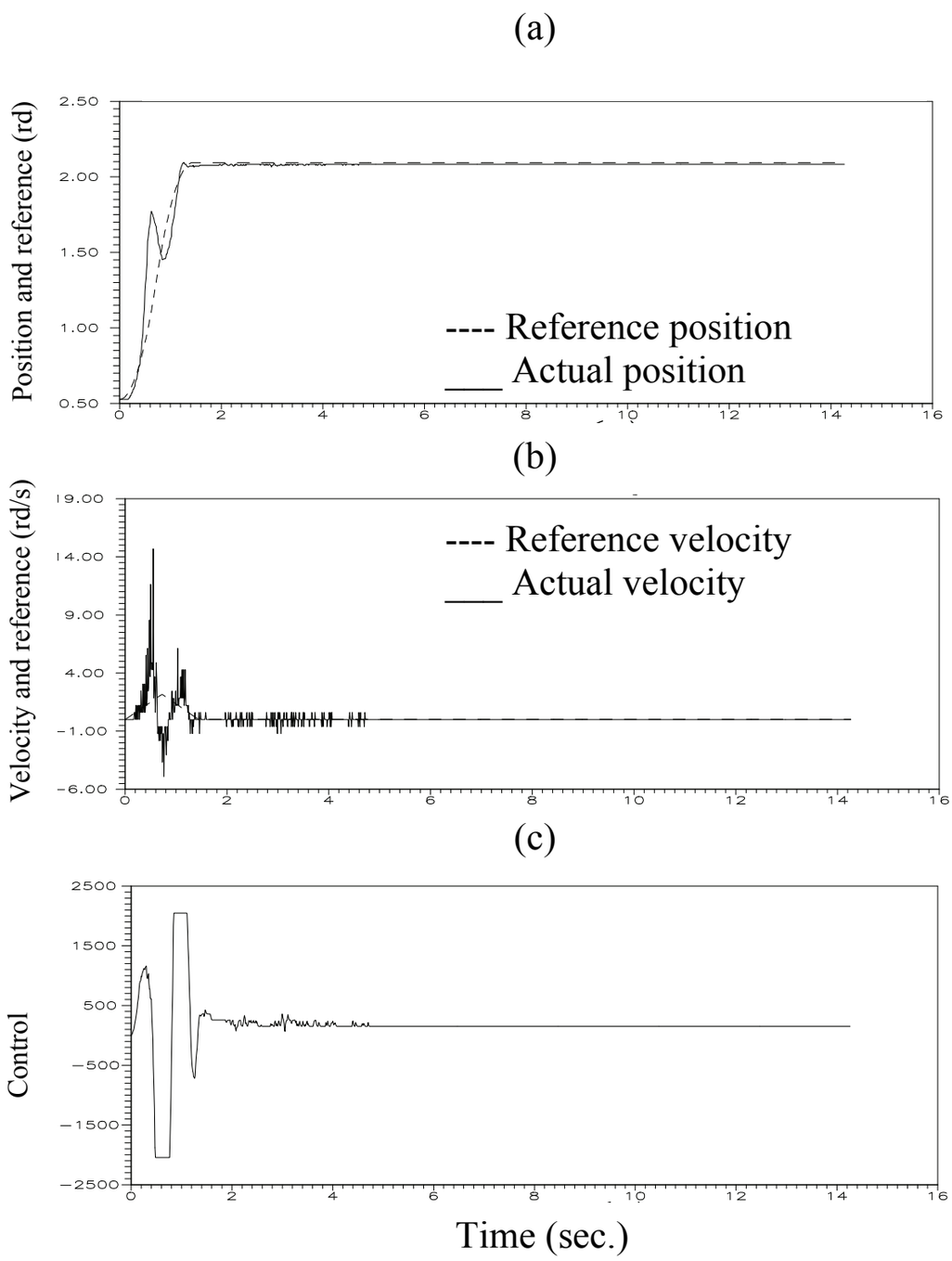

Figure 10. Experimental results obtained in the tracking mode using our proposed GVS2 controller on axis 3 in presence of 900g payload and external disturbance

7. References

Bartolini, G.; Ferrara, A. & Usai, E. (1998). Chattering avoidance by second order sliding mode control, *IEEE Transaction on Automatic Control*, Vol. 43, No. 2, Feb. 1998, pp. 241-246, ISSN: 0018-9286.

Belhocine, M.; Hamerlain, M. & Bouyoucef, K. (1998). Tracking trajectory for robot using Variable Structure Control, *Proceeding of the 4th ECPD, International Conference on Advanced Robotics, Intelligent Automation and Active Systems*, pp. 207-212, 24-26 August 1998, Moscow.

Bouyoucef, K.; Kadri, M. & Bouzouia, B. (1998). Identification expérimentale de la dynamique du robot manipulateur RP41, *1er Colloque National sur la Productique*, CNP98, May 1998, Tizi Ouzou.

Bouyoucef, K.; Khorasani, K. & Hamerlain, M. (2006). Chattering-alleviated Generalized Variable Structure Control for Experimental Robot Manipulators, *Proceeding of the IEEE Thirty-Eighth Southeastern Symposium on System Theory*, SSST '06, pp. 152 – 156, March 2006, Cookeville, TN, ISBN: 0-7803-9457-7.

Fliess, M.(1990). Generalized Controller Canonical Forms for linear and nonlinear dynamic, *IEEE Transactions AC*, Vol. 35, September 1990, pp. 994-1001, ISSN: 0018-9286.

Furuta, K.; Kosuge, K. & Kobayshi, K. (1989). VSS-type self-tuning Control of direct drive motor in *Proceedings of IEEE/IECON'89*, pp. 281-286, November 1989, Philadelphia, PA, 281-286.

Hamerlain M.; Belhocine, M. & Bouyoucef, K. (1997). Sliding Mode Control for a Robot SCARA, *Proceeding of IFAC/ACE'97*, pp153-157, 14-16 July 1997, Istambul, Turkey.

Harashima, E, Hashimoto H. & Maruyama K. (1986). Practical robust control of robot arm using variable structure systems, *Proceeding of IEEE, International Conference on Robotics and automation*, pp. 532-538, 1986, San Francisco, USA.

Levant, A. & Alelishvili L.(2007). Integral High-Order Sliding Modes**,** *IEEE Transaction on Automatic control*, Vol. 5, No. 7, July 2007, pp. 1278 – 1282.

Messager, E. (1992). Sur la stabilisation discontinue des systèmes, *PhD thesis in Sciences Automatiques*, Orsay, Paris, France, 1992.

Nouri, A. S.; Hamerlain, M.; Mira, C. & Lopez, P. (1993). Variable structure model reference adaptive control using only input and output measurements for two real one-link manipulators, *System, Man, and Cybernetics*, pp. 465-472, October 1993**,** ISBN: 0-7803-0911-1.

Sira-Ramirez, H. (1993). A Dynamical Variable Structure Control Strategy, in Asymptotic Output Tracking Problems, *IEEE Transactions on Automatic Control*, Vol. 38, No. 4, April 1993, pp. 615-620, ISSN: 0018-9286.

Slotine, J.J. E. & Coetsee, J.A. (1986). Adaptive sliding controller synthesis for nonlinear systems, *International Journal of Control*, Vol. 43, No. 6, Nov. 1986, pp. 1631-1651, ISSN:0018-9464.

Utkin, V. I. (1992). Sliding mode in control and optimization, Springer-Verlag, Berlin ISBN: 0387535160

Youssef, T.; Bouyoucef, K. & Hamerlain, M. (1998). Reducing the chattering using the generalized variable structure control applied to a manipulator arm, IEE, UKACC, *International conference on CONTROL'98*, pp. 1204-1211, ISBN: 0-85296-708-X, September 1998, University of Wales Swansea.

Robot Manipulators

Edited by Marco Ceccarelli

ISBN 978-953-7619-06-0

Hard cover, 546 pages

Publisher InTech

Published online 01, September, 2008

Published in print edition September, 2008

In this book we have grouped contributions in 28 chapters from several authors all around the world on the several aspects and challenges of research and applications of robots with the aim to show the recent advances and problems that still need to be considered for future improvements of robot success in worldwide frames. Each chapter addresses a specific area of modeling, design, and application of robots but with an eye to give an integrated view of what make a robot a unique modern system for many different uses and future potential applications. Main attention has been focused on design issues as thought challenging for improving capabilities and further possibilities of robots for new and old applications, as seen from today technologies and research programs. Thus, great attention has been addressed to control aspects that are strongly evolving also as function of the improvements in robot modeling, sensors, servo-power systems, and informatics. But even other aspects are considered as of fundamental challenge both in design and use of robots with improved performance and capabilities, like for example kinematic design, dynamics, vision integration.

INTECH
open science | open minds

InTech Europe
University Campus STeP Ri
Slavka Krautzeka 83/A
51000 Rijeka, Croatia
Phone: +385 (51) 770 447
Fax: +385 (51) 686 166
www.intechopen.com

InTech China
Unit 405, Office Block, Hotel Equatorial Shanghai
No.65, Yan An Road (West), Shanghai, 200040, China
中国上海市延安西路65号上海国际贵都大饭店办公楼405单元
Phone: +86-21-62489820
Fax: +86-21-62489821

IntechOpen